

Analysis of the stellar population in the central area of the HII region Sh 2-284[★]

Antonio J. Delgado¹, Anlaug A. Djupvik² and Emilio J. Alfaro¹

¹ Instituto de Astrofísica de Andalucía, CSIC,
Apdo 3004, 18080-Granada, Spain
e-mail: delgado@iaa.es, e-mail: emilio@iaa.es

² Nordic Optical Telescope, Apado 474, 38700 Santa Cruz de La Palma, Spain
e-mail: amanda@not.iac.es

Received April 15, 2008; accepted April 31, 2008

ABSTRACT

Context. There is a lack of state-of-the-art information on very young open clusters, with implications for determining the structure of the Galaxy.

Aims. Our main objective is to study the timing and location of the star formation processes which yielded the generation of the giant HII region Sh 2-284. This includes the determination of different physical variables of the stars, such as distance, reddening, age and evolutionary stage, including pre-main-sequence (PMS) stars.

Methods. The analysis is based on $UBVRcI_C$ CCD measurements of a field of $6.5' \times 6.5'$ containing the cluster, and JHK_s photometry in the $3.5' \times 3.5'$ subfield, centered in the apparent higher condensation. The determination of cluster distance, reddening and age is carried out through comparison with ZAMS, post-MS and PMS isochrones. The reference lines used are obtained from theoretical post-MS and PMS isochrones from the Geneva and Yale groups, for metallicity $Z=0.004$, in agreement with the spectroscopic metallicity determination published for several cluster members.

Results. The results amount to $E(B-V)=0.78 \pm 0.02$, $DM=12.8 \pm 0.2$ (3.6 kpc), $\text{LogAge}(\text{yr})=6.51 \pm 0.07$ (3.2 Myr). The distance result critically depends on the use of low metallicity ZAMS and isochrones. A PMS member sequence is proposed, with an age of $\text{LogAge}(\text{yr})=6.7 \pm 0.2$ (4.7 Myr) which is therefore coeval within the errors with the post-MS cluster age. The mass function for this population in the mass range above $1.3-3.5 M_{\odot}$ is well fitted by a Salpeter mass function. The presence of a different star generation in the cluster with a distinctly older age, around 40 Myr, is suggested. On the other hand, the NIR photometry results indicate a large number of sources with $(H-K_s)$ excess, practically distinct from the optical PMS candidate members.

Conclusions. The analysis of our deep $UBVRcI_C JHK$ photometry of Dolidze 25 therefore reveals a young cluster with coeval MS and PMS populations of age 3.2-5 Myr. In addition, a distinctly older cluster member population of age 40 Myr is suggested. The distance determined for the cluster from quantitative fits to ZAMS and isochrones is distinctly lower than previously published values. This result originates in the consistent use of low metallicity models for ZAMS fitting, applying published metallicity values for the cluster

Key words. open clusters and associations – Dolidze 25 stars: pre-main sequence

1. Introduction

The open cluster Dolidze 25 (06h 45m 06s, $+00^{\circ} 18' 00''$, Epoch 2000) is one of the targets in our long term project on the search for and characterization of PMS members in young open clusters (Delgado et al. 2007, and references therein, DAY-I in the following). The cluster was included in their series of photoelectric studies by Moffat & Vogt (1975) and Moffat et al. (1979). A UBVR CCD photometric study was more recently published (Turbide & Moffat 1993).

In addition to the general objectives of this project (DAY-I), Dolidze 25 presents in principle two additional features of interest. It is located in the Galactic anticenter direction, and has been claimed to have a metallicity distinctly lower than the solar value (Lennon et al. 1990; Fitzsimmons et al. 1992). The cluster is therefore of special interest in our project, because of the ex-

pected finding of PMS stars with low metallicity and possibly at large Galactocentric distances.

The low metallicity of the cluster would contradict the value expected from the published values of the Galactic metallicity gradient. Any of the published values obtained from B-type stars, between -0.05 to -0.07 dex/kpc (Fu et al. 2009), would require too large Galactocentric distances for our cluster to reach the Lennon et al. (1990) metallicity value. On the other hand, recently published results (Przybilla et al. 2008; Przybilla 2008), with an improved method of spectroscopic analysis of B-type stars, suggest a clearly tighter result for abundances of B-type stars in the solar neighbourhood than those found in previous works. The accurate abundances could be considered to define the zero point of B-type stars metallicity at the solar Galactocentric distance, which would imply necessary corrections of previous values towards higher metallicities. We note however, that local metallicity variations with respect to an average gradient have been reported several times (Fu et al. 2009; Pedicelli et al. 2009), and the possible presence of discontinuities and slope changes, especially for large Galactocentric distances are still open. In this

Send offprint requests to: A.J. Delgado

[★] Based on observations made with the Nordic Optical Telescope, operated on the island of La Palma jointly by Denmark, Finland, Iceland, Norway, and Sweden, in the Spanish Observatorio del Roque de los Muchachos of the Instituto de Astrofísica de Canarias.

context, the analysis of cluster parameters, and the eventual improvement of their values is of importance. The cluster was selected as target for one of the COROT¹ Additional Programs (Ripepi et al. 2006). These authors performed VIMOS observations at VLT which revealed the presence of a large number of emission line objects in the region (partial report <ftp://ftp.na.astro.it/pub/astrows06/presetazione-FCUSANO.ppt> at <http://www.na.astro.it/>; <http://earth-sciences.cnes.fr/COROT/A-corot-week.htm>).

Finally, the cluster is located in the center of the giant H-alpha bubble which encompasses the HII region Sh 2-284 (shortened to S284 in the following). Thus the analysis of the stellar content of this field could help to better understand the connection between the star formation processes and the physics of the ionized gas. The S284 region has been the object of a mid-infrared study with Spitzer IRAC bands (Puga et al. 2007). The analysis of these observations (Puga et al. 2009, P09 in the following) includes Dolidze 25, and addresses the properties of massive star formation in the region.

In the present study we report UBVRJHK observations centered in the Dolidze 25 cluster. In the next section we give an overview of the region. In Sect. 3 we describe the different data sets, with reduction procedures. Section 4 presents the optical results and a discussion of the determination of cluster parameters and cluster membership. Section 5 presents the near-IR results and IR-excess sources. Section 6 contains the discussion of the results, and finally the last section resumes the main conclusions.

2. Overview of the region

Dolidze 25 is located in the apparent center of an IR dust bubble (P09). In this article we focus on a photometric study in UBVRJHK of the central Dolidze 25 cluster, and its immediate neighbourhood. In Fig. 1 we show the emission from the 8.0 μm Spitzer/IRAC band (red) obtained from the Spitzer archive and the H α emission (blue) from the AAO/UKST-H α survey (<http://www.roe.ac.uk/ifa/wfau/halpha/>) in a 30' \times 30' area centred on the cluster. The fields covered by the UBVRJ-ALFOSC and the JHK_S-NOTCam images are outlined by a larger and a smaller square, respectively. The projected circular structure is formed by several knots and clouds of H α emitting material, thoroughly discussed in P09. The image suggests a radial connection of several features to the cluster center. We recall here the presence of several arc-like structures, seen to the north and south, and two particularly interesting more defined features. To the north-east we see structures resembling broad arrow peaks, and to the west, a structure which very closely resembles a fore-finger directly pointing to the central cluster, resembling the so-called elephant trunk features observed in some nearby star forming regions. All these structures seem to be geometrically related to the center, the location where Dolidze 25 lies.

3. Observations and models

3.1. UBVRJ photometry

Deep UBVRJ imaging was made with ALFOSC at the 2.6m Nordic Optical Telescope (NOT) during available slots in the nights 25, 26 and 28 of December 2006, and the field was calibrated with photometric standards on the photometric night 21 of February 2007. The detector was a 13.5 μm \times 2024 \times 2024

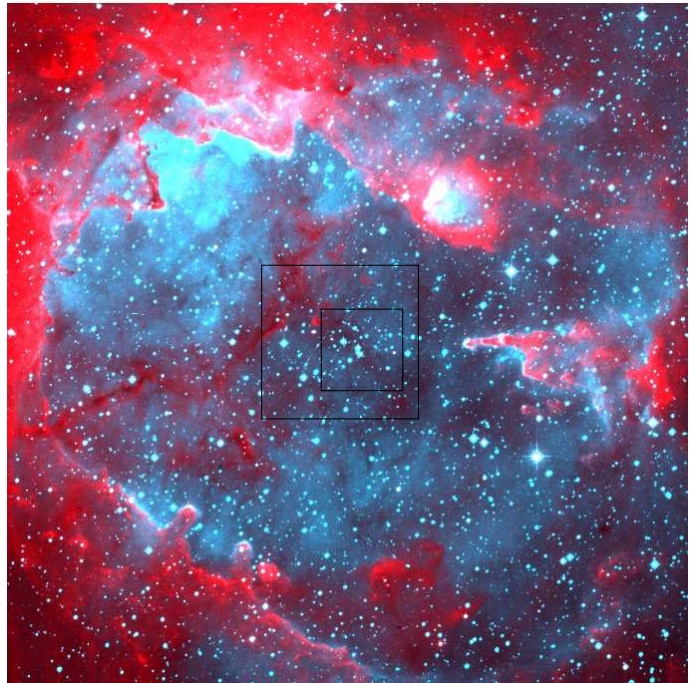


Fig. 1. Colour composite of 30' \times 30' from AAO/UKST-H α survey (blue) and Spitzer/IRAC/8 μm image (red). North up, east left. Dolidze 25 is located in the center of the bubble. In this paper we focus on the central area outlined by the larger and smaller squares representing the coverage of deep UBVRJ and JHK_S photometry, respectively.

pixel back-illuminated E2V CCD, covering a FOV of 6.5' with a pixel scale of 0.19".

The image reduction was carried out with adequate routines in the IRAF package. In every filter both short and long exposure times were secured to cover an as wide as possible brightness range. The long exposure times were 2700, 1800, 1800, 1800, and 3 \times 900 seconds, for UBVRJ, respectively. The final instrumental PSF magnitudes were obtained from the respective frames, computing average values for the stars in common in both exposures. These final magnitudes are then best calibrated by direct correlation to published UBVR observations. In the present case, we used the published CCD UBVR colors (Turbide & Moffat 1993) better than the available photoelectric magnitudes by Moffat & Vogt (1975) which coincide only partially with our field. The $(V - R)$ and $(V - I)$ color indices were calibrated with the catalogued values for 8 standard stars observed in the Landolt (1992) region Rubin149. The uncertainties of our standard indices are calculated as the root mean squared deviations of the averaged O-C values for the different color indices. They amount to 0.05 mag in V , $(U - B)$ and $(B - V)$, 0.01 mag in $(V - R)$ and 0.02 mag in $(V - I)$.

3.2. JHK photometry

Deep near-IR imaging was obtained with NOTCam² at the NOT on the 14 of January 2006. The detector, a 1024 \times 1024 \times 18 μm Hawaii array, the first Science Grade Array for NOTCam (SWIR2), was available in the period October 2005 to May 2006. Its gain was 2.2 e^- /adu and the readout noise 15 e^- . The detector

¹ <http://earth-sciences.cnes.fr/COROT/>

² See URL <http://www.not.iac.es/instruments/notcam/> for details on NOTCam.

Table 1. UBVRJHK photometry of 1673 sources in Do25, sorted on ascending RA. ID is our id number, IDW is the WEBDA id number, and 2MASS is the name of the cross-correlated 2MASS source. Positions are given in decimal degrees and have epoch 2000. One source is listed as an example.

ID	IDW	2MASS	RA	DEC	U-B	σ_{UB}	B-V	σ_{BV}	V	σ_V
	V-R	σ_{VR}	V-I	σ_{VI}	J	σ_J				
	H	σ_H	K	σ_K	MEM	IREX				
1053	16	06450210+0013165	101.2587814	0.22125500	-0.330	0.004	0.601	0.004	13.052	0.003
	0.382	0.008	0.916	0.008	12.014	0.017				
	11.811	0.019	11.730	0.020	1	0				

was found to be linear to within 1% up to 30000 adu, with saturation starting at 54000 adu. About 2% of the pixels were bad, but mainly along the edges of the detector. With this array the zeropoints for NOTCam were 24.02, 23.97, and 23.33 mag (for 1 e⁻/s, and Vega magnitudes) in the bands *J*, *H*, and *K_S*, respectively. We used the wide field camera (0.234"/pix, fov=4") and the broad band filters *J*, *H* and *K_S* with central wavelengths at $\lambda\lambda$ 1.247, 1.632, and 2.140 μ m, respectively, to map the central part of the cluster in a 3 \times 3 dither pattern. Exposing 6 \times 6 seconds \times 9 pointings \times 3 repetitions gave 162 images and a total on-source integration time of 972 seconds per filter.

We used the IRAF package and a set of our own scripts to mask bad pixels, subtract the sky background and flatfield the images using differential twilight flats taken on the same night. After image registration, combination and trimming, the final image size is reduced to 3.5' \times 3.5' (see Fig 6). Point sources were extracted from the final image of each filter using `daofind`, and aperture photometry was made with an aperture radius of the order of the FWHM of the PSF. The flux loss in the PSF wings was corrected for by evaluating an aperture correction for each band on a few bright and isolated stars (with errors < 0.014 mag for all bands). Errors related to flat-fielding were found to be 0.013, 0.012 and 0.015 mag in *JHK*, respectively. The above errors are added in quadrature to the error outputs from the IRAF task `phot` to give conservative measurement errors. We reach down to *JHK* magnitudes of 21.2, 20.0, and 19.5, respectively, with errors < 0.30 mag. The median errors in *JHK* are 0.047, 0.040, and 0.044 mag, respectively, for the whole sample. The limiting magnitudes when requiring the total measurement errors to be < 10%, are 19.7 mag, 18.9 mag, and 18.6 mag in *J*, *H*, and *K*, respectively. We recall that the observations consist of multiple short integrations, obtained in worse than average seeing conditions (FWHM = 0.7" in *K*). We estimate completeness down to at least *J* = 18 mag, *H* = 17.5 mag, and *K* = 17 mag.

The 2MASS point source catalogue (Skrutskie et al. 2006) was used to calibrate both astrometry and photometry, and in regions not covered by NOTCam we used the 2MASS fluxes. We identified 85 common sources and made a plate solution of the NOTCam images with an rms in RA and DEC of 0.15" and 0.14", respectively. All sources were cross-correlated with the 2MASS catalogue using the task `tmatch` with a search radius of 0.5" (> 3 times the rms). The fluxes were calibrated using the 19 stars that satisfy the following three criteria: 1) *K* < 14 mag, 2) have 2MASS ABCD flags, and 3) not being YSO candidates, neither IR-excess sources (see Sect.5) nor optically determined PMS stars (see Sect.4.2.3). The difference magnitudes of these 19 stars (NOTCam - 2MASS) were found to have a standard deviation of 0.06 mag for *J* and *K* and 0.04 mag for *H*. Three bright stars (WEBDA id 15, 17, and 23) have fluxes exceeding the 1% linear range of the detector, and we therefore do not include their NOTCam *JHK* measurements in the table of photometric results.

3.3. On-line table of UBVRJHK photometry.

In Table 1 (only available on-line) we list our photometric UBVRJHK results in the observed fields. Table 1 contains 1673 sources, sorted on ascending RA, and the columns give: Our ID number, WEBDA ID number, 2MASS name, RA, DEC, both in degrees, U-B, σ_{U-B} , B-V, σ_{B-V} , V, σ_V , V-R, σ_{V-R} , V-I, σ_{V-I} , J, σ_J , H, σ_H , *K_S*, σ_{K_S} , MEM, IREX. The column MEM shows membership (1 = young MS and post-MS member, 2 = old MS and post-MS member, 3 = PMS member according to 3 CM diagrams, 4 = PMS member according to 4 CM diagrams); see Sect. 4 for details. The column IREX defines the possible presence of IR excess (0 = no IR excess, 1 = probable IR excess, 2 = bona fide IR excess), for details see Sect. 5.

3.4. Low metallicity ZAMS and isochrones

The low metallicity of Dolidze 25 makes it necessary to consider the consequent changes of the photometric indices. Mainly the value of the absolute visual (*M_V*) magnitude is affected by changes in metallicity, and its variation has been formulated as a linear dependence on metallicity for a given (*B* - *V*) color (Vandenberg & Poll 1989). For the analysis of Dolidze 25, in absence of empirical or semi-empirical ZAMS for metallicities lower than solar, we use theoretical ZAMS and isochrones computed for the corresponding metallicity, and transformed to the observational plane.

In addition to the differences between models, originating in the consideration and treatment of the various physical processes involved in the evolutionary calculations, it is this transformation to observable colors the factor that introduces the largest differences between the different models (Lejeune & Schaerer 2001). To maximize the internal consistency of our results, we adopt reference lines transformed with the same calibration formulae to the observed colors. We use the post-MS Geneva isochrones (Lejeune & Schaerer 2001)³, and the Yale PMS isochrones (Yi et al. 2001) in the Y2⁴ model set, namely those translated to the observational plane with the color transformation by Lejeune et al. (1998). In both cases, the metallicity tracks for Z=0.004, as given for the cluster by Lennon et al. (1990), are used. Neither the Geneva nor the Y2 models contain a nominal ZAMS line. We use here a composite curve, obtained from the Geneva isochrone of age 1000 yr for colors bluer than (*B* - *V*) = 0, and the Y2 isochrone of age 40 Myr for redder (*B* - *V*) color. We refer to this ZAMS line as ZAMS-Z004 in the considerations below. Finally, the Y2 models show that the Color-Color (CC) relation for PMS isochrones deviates from the ZAMS line, specially for spectral types later than B0, a deviation which is larger the younger the isochrone age. The particular (*U* - *B*), (*B* - *V*) relation for each isochrone is then used

³ <http://vizier.cfa.harvard.edu/viz-bin/VizieR?-source=VI/102>

⁴ <http://csaweb.yonsei.ac.kr/~kim/y2solarmixture.htm>

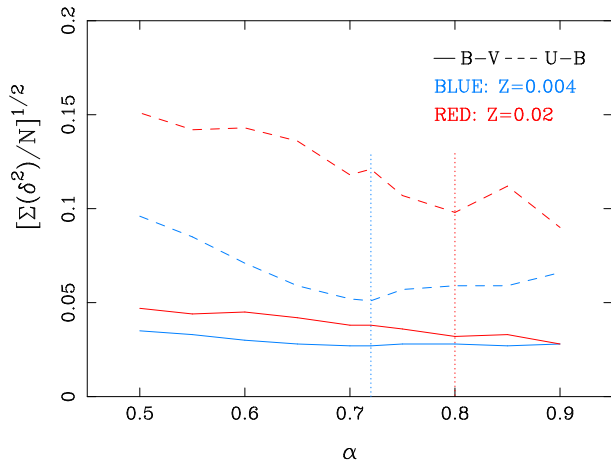


Fig. 2. The variance of ZAMS fitting to unevolved members in CM diagrams is plotted as a function of α . Symbols and color distinguish the results of fitting in the CM diagrams $V, (U - B)$ (dashed lines) and $V, (B - V)$ (continuous lines). Results from fits to solar metallicity ZAMS (red lines) and ZAMS-Z004 (blue lines) are plotted. Vertical dotted lines indicate the minimum variance in both cases.

to compute color excess values, used afterwards in the computation of visual absorption and corresponding distance modulus with respect to this PMS isochrone.

4. Results of UBVR imaging

4.1. Reddening law towards Dolidze 25

As explained in DAY-I, the determination of cluster parameters starts with the selection of bona-fide unevolved MS members, on the basis of the photometric colors, with the help of membership assignments by other authors, and the eventual use of spectroscopic observations. The application of the method requires an assumption of the reddening slope $\alpha \equiv E(U - B)/E(B - V)$ used to shift the stars in the Color-Color (CC) $(U - B), (B - V)$ diagram. Once a reliable sample of non-evolved MS members is selected, they can be used to estimate the absorption coefficient $R_V = A_V/E(B - V)$, appropriate for the extinction law in the direction of the observed field, and to be applied in the calculation of distance modulus.

Turbide & Moffat (1993) derive $\alpha=0.8$ from a simultaneous fit of solar metallicity isochrones to their selected members in the $V, (U - B)$ and $V, (B - V)$ CM diagrams, with distance modulus, age, $E(U - B)$, and $E(B - V)$ as fitting parameters.

We have performed a similar fit, but only to the ZAMS, and selecting stars that can be considered little evolved, constant reddening members. The sample consists of seven stars, five of them among the members by Turbide & Moffat (1993), and our four best candidates to non evolved MS members (actually two of them are in common with the Turbide & Moffat (1993) members sample). Calculations are carried out for ZAMS of solar metallicity (Aller et al. 1982) and of $Z=0.004$ (ZAMS-Z004 described above). Once a reference line and a reddening slope α are chosen, the absolute magnitude M_V , and color excesses $E(B - V)$ and $E(U - B)$ are determined. The average $V - M_V$ and color excesses are used to shift the ZAMS lines in the CM diagrams. For each α , we calculate the quantity $[\Sigma(\delta^2)/N]^{1/2}$, where δ is the distance of every star to the shifted ZAMS in either CM diagram and N is the number of stars. This quantity is plotted versus α in Figure 2. We see in this plot that a minimum is attained for

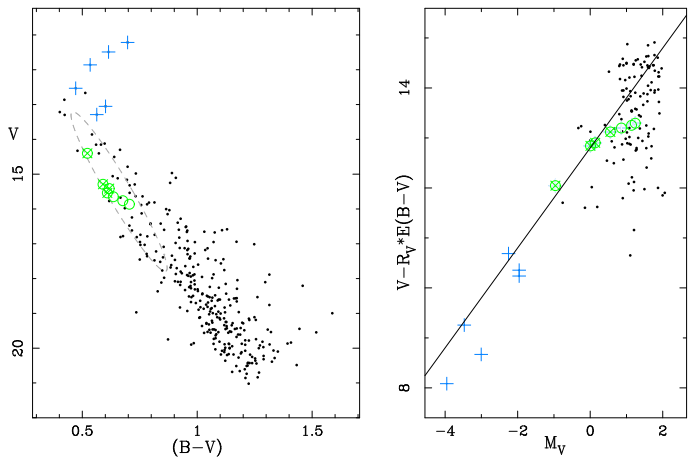


Fig. 3. Selection of upper MS member stars. The left panel shows all stars with measurement in all $UBVRI$ bands plotted in the upper $V, (B - V)$ CM diagram. A dashed line sketches the area where the non-evolved MS members are expected. Stars simultaneously located in similar areas in all four CM diagrams are plotted as circles. In the right panel, $V_0 \equiv V - R_V \times E(B - V)$ is plotted versus M_V for stars brighter than $V=18$. A straight line represents the value $DM=12.8$. As in the left panel, circles represent stars considered as possible unevolved MS members. Among these, crossed circles are the four stars definitely selected as such, for calculation of cluster parameters. Crosses are the assumed post-MS members.

$\alpha=0.72$ when ZAMS-Z004 are used, whereas for the fitting to solar metallicity ZAMS, the result of Turbide & Moffat (1993) would be recovered.

The color excesses of the unevolved MS stars, obtained with $\alpha=0.72$ are then used to calculate $E(V - I)$ from the $(V - I), (B - V)$ CC diagram, and the absorption coefficient $R_V = A_V/E(B - V) = 2.4 \times E(V - I)/E(B - V)$. The result, $R_V=3.10$, coincides with the value characteristic for an average Galactic extinction (Cardelli et al. 1989), and is then adopted, together with $\alpha=0.72$, to calculate color excesses and distances for the cluster stars.

4.2. MS Membership, Distance and Age

4.2.1. Unevolved MS members

To select reliable unevolved MS members we use a method that combines all color indices from $UBVRI$ photometry (DAY-I). Figure 3 illustrates this selection. In the left panel we plot the upper part of the $V, (B - V)$ CM diagram, including all stars with measured values in all five $UBVRI$ bands. A dashed-line ellipse describes the region of the diagram where the non-evolved MS cluster members are expected, if any. The simultaneous location of stars inside similar regions in all four CM diagrams, together with their consistent location in the CC diagram, results in the sample, marked with circles in both panels of Fig. 3.

In the right panel, we represent the quantities $V - R_V \times E(B - V)$ versus M_V , only for stars brighter than $V=18$, to make the plot clearer. A straight line for $DM=12.8$ is plotted as an indication. In this right panel we observe the presence of foreground and background star groups, respectively, below and above the distance modulus value described by the selected unevolved MS members. Three of these appear to have a relatively lower distance modulus, and are further rejected. The final sample considered for the calculation of cluster distance modulus are those

stars plotted as crossed circles. In both plots, crosses represent the stars adopted as post-MS members (Moffat et al. 1979; Turbide & Moffat 1993), to be considered in principle for the estimation of post-MS age.

4.2.2. Color excess, distance, and post-MS age

The average values and rms deviations of color excess and distance modulus for the unevolved MS members amount to $E(B-V)=0.78\pm 0.02$, $DM=12.8\pm 0.2$. They are used as reference values to estimate membership for the remaining stars, following the procedure explained in detail in DAY-I.

An estimate of the post-MS cluster age is obtained from the comparison to post-MS isochrones, where we use the set of models from the Geneva-isochrones for $Z=0.004$ and solar mixture. The comparison is illustrated in Fig. 4, where the upper CM diagrams $V, (U-B)$, $V, (B-V)$, $V, (V-R)$, and $V, (V-I)$ are plotted, with indication of the selected unevolved MS- and post-MS members (See. Fig. 2). To avoid the possible influence upon these diagrams of binarity (Golay 1974) or emission lines (Mermilliod 1982), we restrict our comparison to the two stars marked with crossed squares in the figure. A quantitative estimate, with extrapolation in each diagram to the age values which would exactly reproduce the locations of both stars, gives 8 formal age values, one for each star in every one of the four CM diagrams. The average, and rms deviation of these values amount to $\text{LogAge}(\text{yr})=6.51\pm 0.07$, or 3.24 ± 0.5 Myr, in good agreement with age values (3.8 Myr) for Dolidze 25 and its associated HII region, quoted in P09.

We note the significant difference between our distance result, and the published distances for the cluster, around $D=5.3$ kpc (Moffat & Vogt 1975; Turbide & Moffat 1993), a difference which originates mainly in the use of low metallicity ZAMS in the distance estimate.

The effect of metallicity changes upon the cluster distance was discussed by Turbide & Moffat (1993), considering the expected variations due to a Galactocentric metallicity gradient. The key point here is however the low metallicity value obtained by Lennon et al. (1990), $Z=0.004$, which does not follow the predictions of any gradient, as mentioned above. The question actually concerns absolute abundances rather than relative ones. We recall in this context the results by Przybilla et al. (2008), who obtain a much tighter results than previous works for B-type stars abundances in the solar neighbourhood. These results suggest that previous metallicity measurements are systematically too low, but the precise value of this offset and its application to stars located far outside the Solar radius is not clearly established. We therefore prefer not to adjust the metallicity value. We note that a "best guess" offset would change our distance estimate from 3.6 to 4.0 kpc and leave the rest of our conclusions essentially unchanged.

4.2.3. PMS Membership and Age

The remaining stars are now studied on the basis of the adopted values of distance and color excess. The method has been explained in detail in DAY-I. It consists in comparing color excesses and distance moduli of each star with the average values obtained for the unevolved MS members. Distances are measured with respect to ZAMS and with respect to PMS isochrones from the Y2 set, for metallicity $Z=0.004$, and ages from 1 to 10 Myr. In this way, each star has assigned several pairs of values of color excess and distance, and is considered either MS or PMS

member, when one of these pairs agrees with those obtained for the unevolved MS members. Photometric uncertainties are considered in this assignment, and allowance is made for color excesses well above the average of the values for unevolved MS members (see DAY-I).

From these comparisons, a star can be assigned as member with respect to several PMS isochrones, whose mean age value provides an age estimate for the PMS candidate. The age and uncertainty of the candidate PMS sequence is then obtained from the average value of the ages obtained for all candidates, and its rms deviation. This operation results in the value $\text{LogAge}(\text{yr})=6.7\pm 0.2$. The observed PMS sequence seems therefore to be coeval with the more massive MS members, in contrast with evidence found in other young clusters (Delgado et al. 2004, 2006, 2007, and references therein), where both cases of PMS sequences younger and older than the corresponding MS members are found.

5. Results of the JHK_S imaging

5.1. Near-IR excess sources

The $J-H/H-K$ diagram for 651 sources in the $3.5'$ field of deep JHK imaging with NOTCam (see Fig. 6) is shown in the left panel of Fig. 5. The loci of main-sequence, giant and supergiant stars (Koorneef 1983) are indicated with bold curves. A reddening slope of $E(J-H)/E(H-K) = 1.6$ is calculated based on the NOTCam JHK_S filter passbands (cf. Sect. 3.2) and using the $A_\lambda \propto \lambda^{-1.7}$ parametrization of the near-IR extinction law (Whittet 1988). The majority of the sources are clustered around the loci of main-sequence and giant stars, and only marginally displaced along the reddening vector, in agreement with the average low extinction over this area as estimated in Sect. 4.1 ($A_V = 2.4$ mag, $A_K = 0.24$ mag).

Sources located to the right and below the reddening line in the $J-H/H-K$ diagram - i.e. the above calculated reddening vector fixed for an A0 star - have excess emission in the near infrared. In order to account for the uncertainties in the observed colours, we define as *bona-fide* IR-excess sources those located in this area and separated from the reddening vector by more than 2σ of the individual errors in the colour indices $J-H$ and $H-K$ (see Sect. 3.2). Those sources that are separated from the reddening vector by a distance between 1 and 2σ only are designated *probable* IR-excess sources. For the $3.5' \times 3.5'$ deep field we extract a sample of 29 bona-fide and 26 probable IR-excess sources. With this relatively conservative criterium we will not sample all the IR-excess sources. Because deep JHK_S imaging was obtained in only part of the $6.5' \times 6.5'$ field studied in the optical (see Sect. 4), we have used the 2MASS point source catalogue to search for IR-excess sources. Using the same near-IR extinction law as above, the reddening slope $E(J-H)/E(H-K)$ becomes 1.78 because of the slightly different JHK_S filter passbands for the 2MASS survey at $\lambda\lambda$ 1.24, 1.66, and $2.16\ \mu\text{m}$, respectively. The $J-H/H-K$ diagram for the 310 sources with ABCD flags is shown in the right panel of Fig. 5. We have applied the same selection criterium for near-IR excess as above. For the $6.5' \times 6.5'$ field we find using 2MASS a total of 8 bona-fide and 20 probable IR-excess sources. In this diagram we also mark those cluster members found from optical photometry that have IR-excesses. In both samples the fraction of IR-excess sources with respect to total number is about 8-9%.

The 55 IR-excess sources found in the deep NOTCam field are in the magnitude range $12.6 < K < 19.2$ with an average at $K = 17.1$ mag, and only 5 of these have 2MASS counterparts.

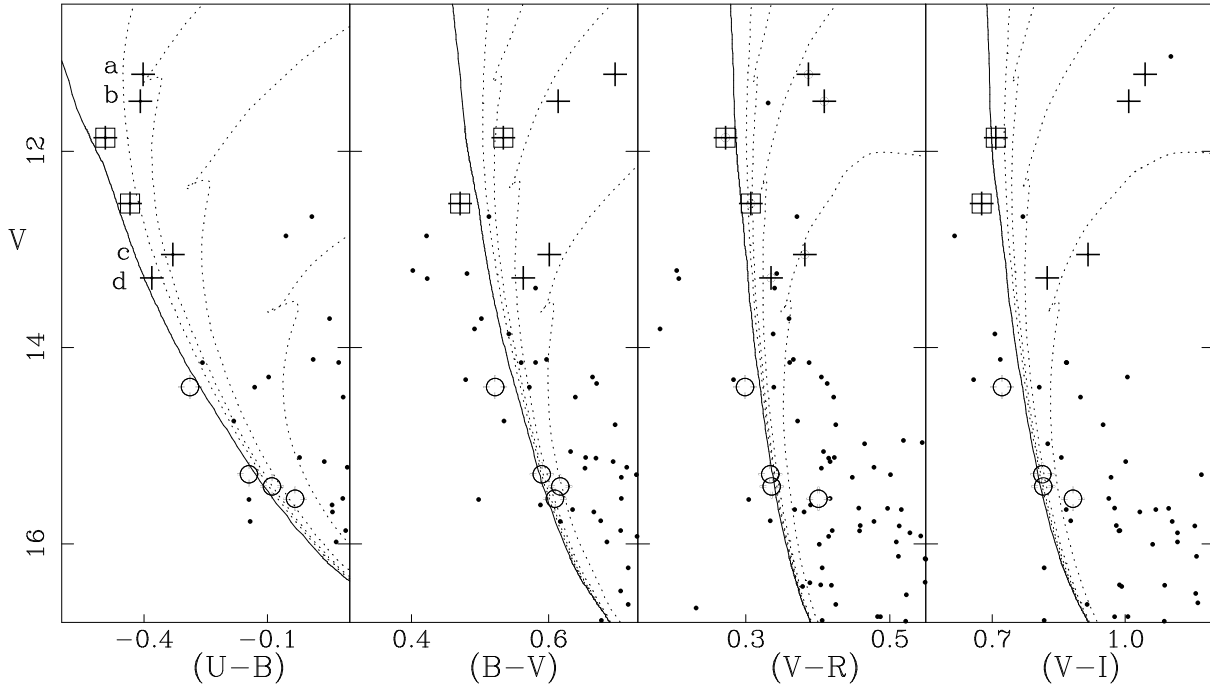


Fig. 4. Comparison of upper cluster sequence to isochrones in the CM diagrams. The ZAMS line for $Z=0.004$ (continuous line. See text) and Geneva isochrones for the same metallicity and $\text{LogAge}(\text{yr})$ 7.0, 7.2, 7.5 and 8 (dotted lines, from left to right in each panel) are plotted. Circles are stars adopted as unevolved MS members. Crosses are stars adopted as post-MS members. Among them, crossed squares are those stars considered to estimate the age. The position of stars labeled $a - d$ is commented in the text. A quantitative comparison (see text) gives $\text{LogAge}(\text{yr})=6.51 \pm 0.07$ for the post-MS cluster age.

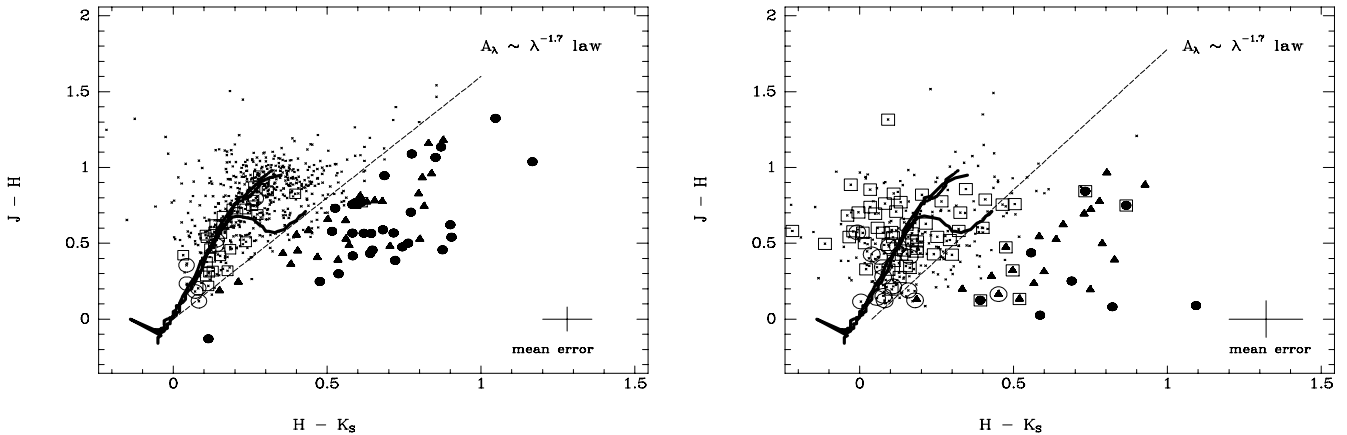


Fig. 5. The $J-H/H-K$ diagrams for the two near-IR datasets used. **Left:** The $3.5' \times 3.5'$ central part of Do25 with deep NOTCam imaging and a total of 651 sources. **Right:** The 310 2MASS point sources with ABCD flags found in the $6.5' \times 6.5'$ field of our optical study. **Both diagrams:** The bold curves outline the loci of main-sequence and giant stars. The reddening vector of an A0 star is shown as a dashed line. Bona-fide IR-excess sources (filled circles) are located more than 2σ of the individual errors in $J-H$ and $H-K$ to the right and below the reddening line. Probable IR-excess sources (filled triangles) are those separated by between 1 and 2σ only. The optically selected cluster members from Sect. 4 are marked with large open circles (MS stars) and large open squares (PMS stars) for reference.

Among these 5 only 2 have IR-excess according to the 2MASS dataset. The remaining 3 have failed to be detected as IR-excess sources in the 2MASS dataset. It is reasonable that the shallower 2MASS survey detected fewer excess sources since the individual errors in the colours are larger. Only 9 of the total of 28 2MASS IR-excess sources are located inside the NOTCam deep field. These are in the magnitude range $12.6 < K < 15.5$ and are all optically visible sources. Surprisingly, it may seem at first, that only two of them are confirmed to be IR-excess sources with

the deeper NOTCam photometry. Looking in detail at the colour indices we find that for all the 7 “non-confirmed” sources, the $J-H$ and $H-K$ indices vary by 0.25 - 0.6 mag between the two epochs Nov-1999 for 2MASS data and Jan-2006 for NOTCam data. (For sources without IR-excesses the median of the absolute differences between the two datasets is < 0.07 mag in the colour indices.) It is also worth mentioning that 3 of those 7 “non-confirmed” IR-excess sources are optically selected cluster members (see Sect. 4).



Fig. 6. RGB image of the NOTCam deep JHK_S imaging of the $3.5' \times 3.5'$ central part of Dolidze 25. North up, east left.

We consider it a sufficient condition for an IR-excess source to have measurable IR-excess in one of the epochs, and we conclude that the combination of NOTCam and 2MASS data yields a total of 81 IR-excess sources (55 from NOTCam plus 28 from 2MASS minus 2 overlapping). Thus, the lack of overlap between the two sets of IR-excess sources is explained in terms of sensitivity difference (i.e. difference in error bars) and most importantly: intrinsic source variability. Variability is expected for young stars and is often used as a criterium of stellar youth; see e.g. Kaas (1999) for a study of the efficiency of this criterion compared to that of IR-excess for membership assignment in a young embedded cluster.

5.2. Cluster membership of near-IR excess sources

The excess emission in the near-IR is attributed to thermally radiating hot circumstellar dust. Determined by the temperature distribution of the dust particles, a superposition of blackbodies is produced, giving an excess flux at IR wavelengths compared to the spectral energy distribution (SED) of a naked star. Whether the dust is spatially distributed in a disk (typical for Classical T Tauri stars) or more spherically distributed (typical for protostars) is reflected in the shape of the SED towards the mid-IR. With only $UBVRIJHK$ photometry for this region we can not say much about the distribution of the dust, only its possible presence. Because the typical number fraction of protostars with respect to PMS stars with disks is about 1/10 in young clusters, we statistically expect our population of IR-excess YSOs to be dominated by Class II sources. We can not exclude, however, that some of our IR-excess sources may be protostars of Class I type.

In Fig. 7 we plot the K band histogram of all our observed sources in the deep $3.5' \times 3.5'$ field as well as that calculated from the Besançon model of our Galaxy (Robin et al. 2003). In order to compare these numbers to the expected K -band counts of extragalactic origin, we have used the average values of the

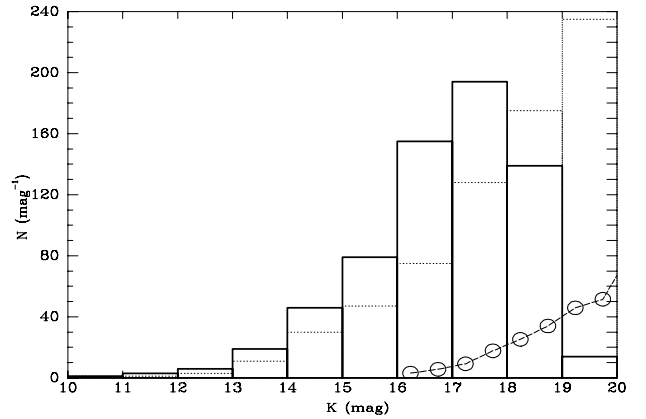


Fig. 7. K -band histogram of all sources in the $3.5'$ field (continuous histogram) compared to the histogram of K -band counts according to the Besançon Galaxy model (dotted histogram). Circles show the number of extragalactic sources (Table 4 in Barro et al. (2009)) scaled to our field size and corrected for a cloud extinction of $A_K = 0.24$ mag.

deep fields presented in Table 4 of Barro et al. (2009). Their numbers were scaled down to the size of our field and corrected for cloud extinction ($A_K = 0.24$ mag) by shifting the values a quarter of a bin size to the right. From the figure it is evident that our observations are complete to around $K = 17.5$ mag. The level of extragalactic contamination in this bin is only $\sim 7\%$ and can not explain the excess of observed compared to model counts. In the magnitude range $18 < K < 19$ mag, however, it is possible that $\sim 20\%$ of our source detections are distant galaxies.

How the above percentages translate to percentages in the IR-excess sample is not obvious. Examining the map of cluster member candidates, however, we find that the faintest IR-excess sources are preferentially located in the central part of the image following the higher spatial density in general. Thus from the spatial distribution it is unlikely that the IR-excess sample in the magnitude range $17 < K < 19$ consist of extragalactic sources, but we note that although we list our 81 IR-excess sources from Sect. 5.1 as YSO candidates, in the faintest bins there is a probability of extragalactic contamination possibly of the order of 10-20%.

5.3. Comparison with optically selected cluster members

A total of 104 pre-main-sequence (PMS) members were found in the $6.5' \times 6.5'$ area covered by our $UBVRI$ photometry (see Sect. 4.2.3). There are 2MASS counterparts with ABCD flags in all bands for 57 of these, of which only 5 have IR excess (see right panel of Fig. 5). Thus, less than 10% of the optically selected PMS members that are also detected in JHK with 2MASS, are found to exhibit excess emission in the near-IR. Inside the $3.5' \times 3.5'$ small deep field there are 31 optically selected PMS stars of which only 3 have IR excess.

Only 19 of the 62 IR-excess sources are optically visible in the V band - a necessary condition for our optical PMS selection. There are only 3 sources with both PMS and IR-excess classification in this field (these have ID numbers 468, 903, and 1563 in Table 1). Thus only 3/19 or 16% of the IR-excess sources that are optically visible are classified as PMS members in our optical study. It is clear from the left panel of Fig. 5 that practically all optically selected PMS stars are found quite near the loci of

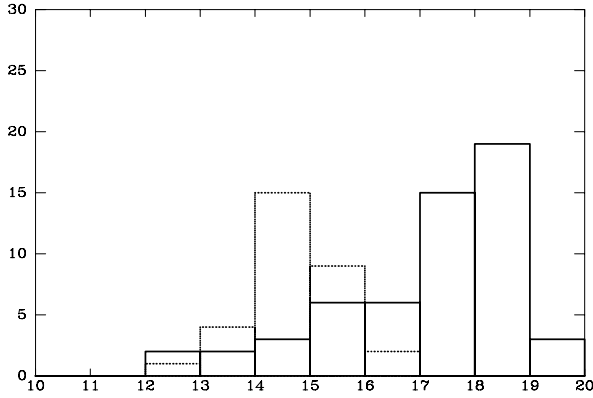


Fig. 8. Left: K-band histogram of the two samples of young cluster member candidates: optically selected PMS stars (dotted line) and IR-excess sources (continuous line).

main-sequence stars in the $J-H/H-K$ diagramme and definitely to the left of the reddening line.

The fact that most of the optically selected PMS stars are found without signs of optically thick circumstellar disks, is either because they are so evolved (or independently of age they have lost their circumstellar material), or the IR imprints of the disks are not detectable in the near-IR. It is well known from mid-IR studies (e.g. Kaas et al. 2004) that only about 50% of the IR-excess sources in young embedded clusters show up with excesses in the $J-H/H-K$ diagramme. In the case of Dolidze 25, which is not really embedded, it is possible that only around 16% of the optically visible PMS stars have disks, but this can only be assessed using mid-IR photometry.

Using two different photometric methods we have two samples of PMS cluster members with very little overlap. The optically selected PMS stars have a magnitude range of $12.6 < K < 16.6$, i.e. all being relatively bright in the near-IR. The near-IR excess sources on the other hand span the larger magnitude range $12.6 < K < 19.2$ with a median at $K = 17.8$ mag. Thus, in general they comprise a fainter population, see Fig. 8. Correcting for average extinction ($A_K = 0.24$ mag) and distance ($DM = 12.8$ mag) we get absolute magnitudes from $-0.4 < M_K < 6.2$ mag for the IR-excess sources. Assuming a typical age of 2-3 Myr for the IR-excess sources, the sub-stellar limit is around $M_K = 5.5$ mag according to PMS evolutionary tracks (Baraffe et al. 1998). The mass range of the IR-excess population extends thus to well beyond the brown dwarf limit, while our completeness estimate at $\sim K=17.5$ mag corresponds to $M_K=4.5$ mag only.

This statistical result shows that the optical photometric method and the near-IR excess method sample different PMS populations, possibly with an age difference, but not necessarily so. The multi-wavelength approach covering both optical and near-IR bands in photometric studies of clusters is advantageous because the two methods are complimentary. This same conclusion was drawn from a similar type of study of the double cluster in Sh2-294 (Yun et al. 2008).

6. Discussion

6.1. Characteristics of the Dolidze 25 cluster

A deep UBVRIJK photometric study of the Dolidze 25 cluster, in a $6.5'$ field centred around the B1 stars TYC 148-2558-

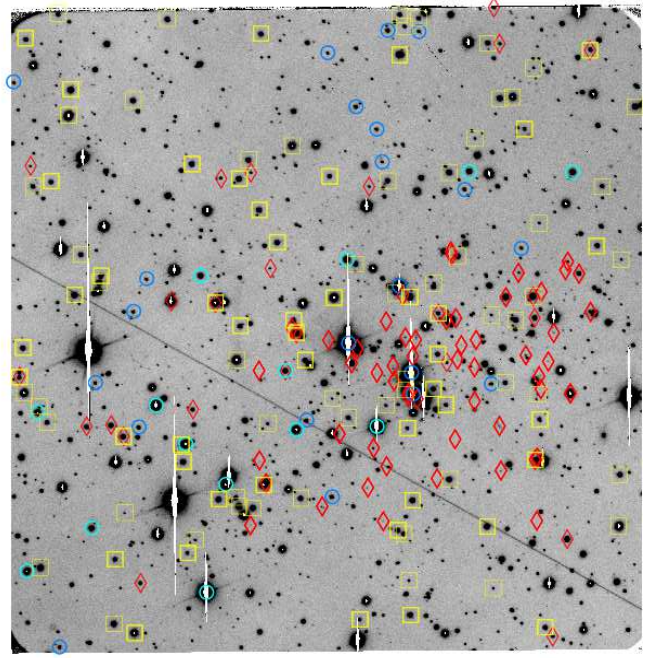


Fig. 9. ALFOSC R-band image of the $6.5' \times 6.5'$ area (north up and east left). The location of MS and post-MS stars of the younger generation (cyan circles) and of the older generation (blue circles), optical PMS candidates (yellow squares), and IR-excess sources (red diamonds) are shown. Note that the IR-excess source selection has a higher sensitivity in the smaller $3.5' \times 3.5'$ area covered by NOTCam.

1 and TYC 148-2577-1, SIMBAD names for our ID 1060 and 1362, i.e. WEBDA 17 and 15 (Moffat et al. 1979), is presented in the previous sections. This field covers an area of almost 7×7 pc, using our new distance estimate of 3.6 kpc described in Sect. 4.2.2. The analysis of cluster membership resulted in a total of 214 candidate cluster members: 35 main-sequence (MS) and post-MS members, 104 optically selected pre-main sequence (PMS) members, and 81 IR-excess sources, probably young PMS stars with circumstellar disks (Class II sources), although Class I sources can not be excluded. Six of the IR-excess sources coincide with optically selected PMS stars.

6.2. Age estimates

The membership analysis of the central Dolidze 25 cluster shows a young generation of stars, of around 3-5 Myr, with a rich population of PMS candidate members, coeval to the upper massive MS stars. However, this analysis also reveals the presence of older stars, which are selected as MS members of lower mass and luminosity than the selected PMS candidates. This suggests the presence in the cluster of two generations of stars. In this hypothesis, the four member stars labeled with *a* to *d* in the left panel of Fig. 4, can be interpreted as the evolved upper sequence of the older star generation. To illustrate this point we show a comparison in Fig. 10, where the $V, (B-V)$ diagrams of these suggested generations are plotted separately.

The main indication that supports this suggestion is the presence of low mass MS candidate members, together with the very good visual fit of the older isochrone to the redder post-MS stars. A formal age calculation for the older post-MS stars in the right panel of Fig. 10, performed in the way explained in Sect. 4.2.2,

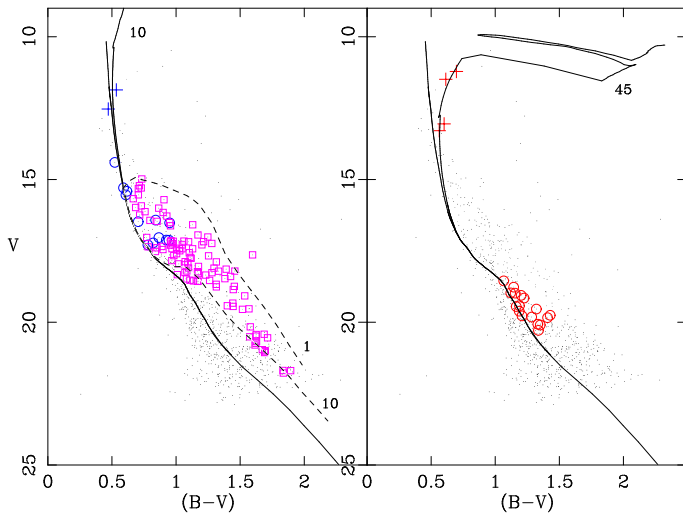


Fig. 10. $V, (B - V)$ diagrams with indications in the cluster members assigned to two generations of stars at different ages. In both panels, all stars are represented with small dots. In the left panel, proposed young members (3-5 Myr) are plotted, with post-MS (crosses) and MS members (circles), and PMS members assigned in at least 3 CM diagrams (squares). Cluster members in the older generation are plotted in the right panel, with the same meaning for the symbols. ZAMS-Z004 line (continuous thick), 10 Myr isochrone (continuous thin), and PMS isochrones of ages 1 and 10 Myr (broken) are plotted and labeled in the left panel. The same ZAMS, and the 45 Myr isochrone are plotted in the right panel.

gives $\text{LogAge}(\text{yr}) = 7.6 \pm 0.2$. On the other hand, MS candidate members in the V range 16-18 mag could belong to both generations, and some of them could indeed be PMS stars approaching the MS. Even some of the faint MS members ($V > 18$), namely those with redder $(B - V)$ index (Fig. 10, right panel), could also be the last signs of a PMS sequence in the older star generation. The precise status of each star cannot be ascertained here, since all candidate members are at the same distance, and with comparable color excess: these are actually the criteria to propose them as cluster members. A detailed spectroscopic study, aiming at the simultaneous determination of spectral type and radial velocity for these stars (Delgado et al. 1999, 2004) is planned as the appropriate tool to confirm the suggested age structure.

In this context we remark that the indications of age spread, and sequential or continued star formation in young clusters are widely reported in the literature (i.e. Subramaniam et al. 2006; Bhavya et al. 2007; Delgado et al. 2007, and their references). Evidence of episodic, and sequentially triggered star formation, has been suggested in large forming regions of the Small Magellanic Cloud (Sabbi et al. 2007; Carlson et al. 2007), and NGC6946 (Larsen et al. 2002; Sánchez Gil et al. 2009). The interesting point in the present case, if confirmed, is the presence of two star generations in the same place.

The interpretation of the stars labeled $a - d$ in Fig. 4 as evolved cluster members requires some comments. Their location in the $V, (V - R)$ and $V, (V - I)$ CM diagrams supports this hypothesis, which is however contradicted by the position of the stars in the $V, (U - B)$ CM diagram (see Fig. 4). In this last diagram, the comparison to isochrones under the assumption that they are evolved cluster members, suggests an age of at most 15 Myr. One possibility to solve the discrepancy is to assume that they indeed are as young as indicated by their $(U - B)$ color,

Table 2. The 35 MS and post-MS members found in our analysis of a 6.5' wide field. The last column indicates the age group, where old means around 40 Myr and young 3-5 Myr. For fluxes, colours and coordinates we refer to Table. 1 (available on-line only).

ID	WEBDA	2MASS	V (mag)	Age group
298		06445568+0015307	17.034	young
513			19.839	old
649			19.756	old
761		06445984+0015311	17.128	young
786			19.152	old
1022			19.775	old
1053	16	06450210+0013165	13.052	old
1060	15	06450217+0013294	11.490	old
1121	18	06450266+0014218	13.290	old
1179			18.549	old
1214			20.284	old
1243	19	06450356+0012569	12.532	young
1244			19.611	old
1329			19.058	old
1362	17	06450471+0013472	11.215	old
1371	197	06450477+0014379	16.479	young
1422	196		18.772	old
1441			20.068	old
1522			18.971	old
1560	123	06450680+0012549	15.539	young
1609	119	06450726+0013306	17.292	young
1863	110	06450966+0012217	15.291	young
1930	22	06451043+0011164	11.861	young
1943	174	06451066+0014281	17.221	young
2003	107	06451127+0012463	15.414	young
2095	102	06451246+0013096	14.402	young
2130			19.816	old
2157			18.982	old
2188			19.422	old
2289			19.450	old
2308		06451507+0011553	17.121	young
2423		06451636+0010433	19.538	old
2499		06451724+0013054	16.519	young
2533		06451767+0011292	16.421	young
2581			20.097	old

while the other three color indices would just reveal, either simple reddening, with a peculiar reddening slope, or some color excess, which increases towards redder indices.

In the line of considering these stars younger than proposed here, we might recall recent results on massive young clusters, where the presence of a noticeable supergiant population is argued (Clark et al. 2009; Alexander et al. 2009). The assumption that the brightest stars in our CM could indicate such a population would result in a distance from them around 7 kpc, which would discard them as cluster members, even under consideration of the largest distance estimates given for Dolidze 25 in the literature.

On the other hand, the presence in these stars of color excesses which are larger for redder colors is also uncertain. It is in any case contradicted by our NIR results, in which none of the proposed post-MS candidates appear to exhibit NIR excess (see Sect. 5). This lack of NIR excess also weakens the suggestion of a redder binary companion which would show up in redder color indices. The performance of adequate spectroscopic observations is needed to elucidate among these possibilities, including the one put forward here, which considers the presence of two generations of stars in the cluster.

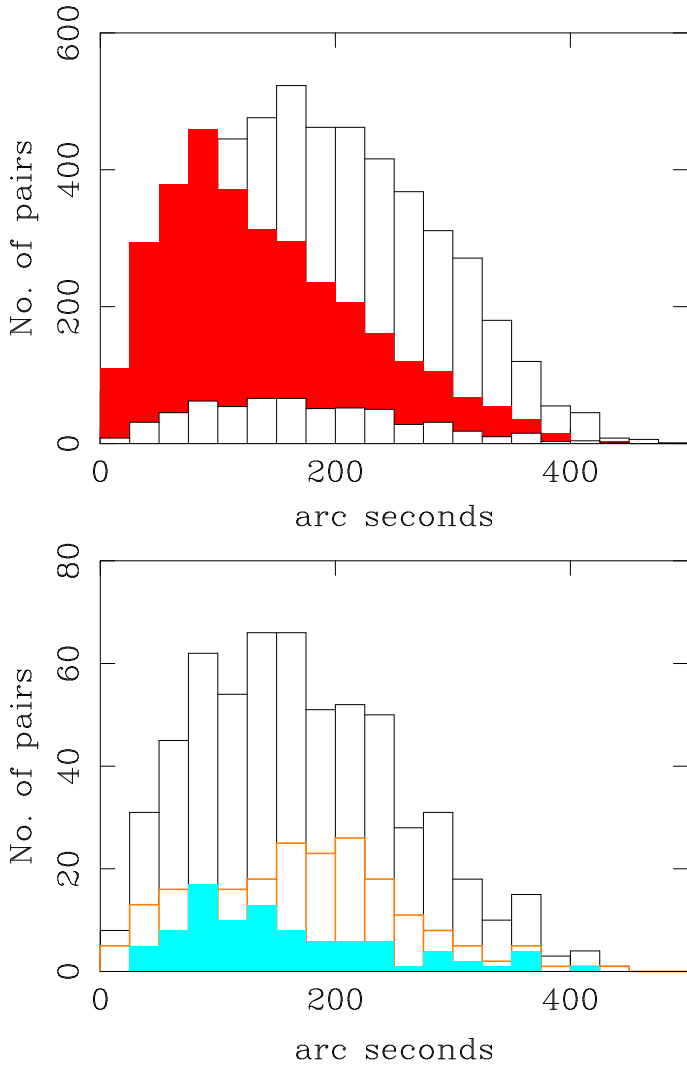


Fig. 11. The number of pairs as a function of separation (in arc seconds), a measurement of the clustering properties of a population, is shown in histograms. **Top:** The optically selected PMS stars comprise the large population in the white/open histogram, the IR-excess sources are shown as red/filled histogram, and the total population of MS and post-MS stars in the small white/open histogram. **Bottom:** The total MS and post-MS population is shown in the white/open histogram, the older population in the orange/bold line histogram, and the younger population in the blue/filled histogram.

6.3. Spatial distributions

The spatial distribution of the various cluster members is shown in Fig. 9, overlaid on an R-band image, the different colours and symbols distinguishing different populations. The MS and post-MS members have a clear zone of avoidance towards the south-west, otherwise they are few and relatively scattered. The IR-excess members seem to have a preference along a SE-NW diagonal belt with an enhanced surface density around ID 1362, which appears to be at the approximate cluster center (see also Fig. 6, the area over which we have deep JHK_s imaging). There is an enhanced number density of sources both in the optical and near-IR images along the SE-NW diagonal belt. There seem to be no apparent spatial preference among the optically selected PMS stars.

We calculate the distribution of separations of pairs of members within the different sub-groups, a way to quantitatively assess possible clustering properties (Kaas et al. 2004), although projected in the plane of the sky. In Fig. 11 we show in histograms the number of pairs versus separation (in arc seconds). Strong peaks in this distribution indicate the scale of clustering or sub-clustering of the population, or more correctly: the approximate size/diameter of the densest region. The upper panel shows the distribution of pairs of optically selected PMS stars (largest group), IR-excess sources (medium group), and all MS and post-MS sources (small group). For the optically selected PMS stars there is a small peak around $160''$, translating to about 3 pc using our distance estimate of 3.6 kpc, but the distribution is broad and indicates that the optically selected PMS stars are in general quite scattered. The IR-excess sources, on the other hand, have a much more pronounced peak, located at $90''$ or 1.6 pc. We —bf note that the deep near-IR study was made in a smaller field, and only the shallower 2MASS survey could be used for the whole area, such that the histogram should not be considered beyond $210''$ for this group. There seems to be a clear tendency of clustering of this population.

The MS and post-MS population, which is a comparatively small group, is seen to have a relatively flat distribution in the upper panel. When separating the total MS and post-MS population into the two age groups suggested in the previous section (approximately 5 Myr and 40 Myr), we see that the spatial distribution of the two is distinct. The younger generation (blue/filled histogram) is slightly more clustered, i.e. the distribution peaks at a smaller scale, than the older generation (orange/bold line histogram). The young generation of MS and post-MS stars peaks around the same scale as the IR-excess population.

Although the number statistics is relatively small, this gives an independent support to the hypothesis of two different generations of MS and post-MS stars suggested by isochrone fitting and described in Sect. 6.2. The spatial distribution of a cluster population is expected to become more dispersed with time. Assuming a typical stellar velocity dispersion of $\ll 1.5 \text{ km s}^{-1}$ found for old ($> 10^8 \text{ Myr}$) open clusters (Lohmann 1972), one might expect 40 Myr old stars to have moved quite some distance away from their birth place. We also note that much larger velocity dispersions have been found for the young clusters NGC2244 and NGC6530 of 35 and 8 km s^{-1} , respectively (Chen et al. 2007). Thus, part of the older population could be located outside the 7 pc wide field studied by us, but only a proper motion study will reveal the velocity dispersion in Dolidze 25.

6.4. Mass function

The quantitative measurement of ages described in Sect. 4.2 above, provides mass estimates for the assigned cluster members, both from the ZAMS and post-MS isochrones, and from the PMS isochrones as well. These mass values are averages of the values read from the corresponding reference lines, and are calculated in the same way as the age estimates.

We apply here these calculated mass values to illustrate the properties of the cluster mass function. In Fig. 12 we plot the logarithm of the number of stars of mass value versus the logarithm of the star mass, in units of solar masses. The break down of the function at masses below 1.3 solar masses is probably due to an underabundance of low mass stars, but other factors, such as the incompleteness of the detected sample should be present, and we do not discuss further this feature. On the other hand, the over abundance of massive stars is probably due to the consideration of all MS and post-MS stars in this function, without dis-

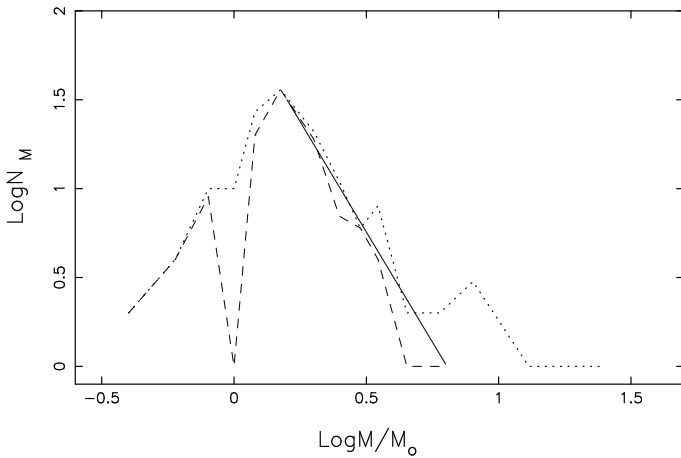


Fig. 12. Mass function for the candidate members in Dolidze 25. The models of Lejeune & Schaerer (2001) and Yi et al. (2001) for $Z=0.004$ have been used to estimate membership and calculate masses for the assigned members. Mass functions of PMS candidates (dashed curve) and all members (dotted curve) are plotted. The continuous straight line reproduces the slope of the Salpeter IMF (-2.35), which is seen to fit very well the calculated mass function for PMS candidates of masses above $\text{Log}M/M_{\odot}=0.2$.

tion of the argued presence of two different star generations. In fact, no differences in mass function depending on metallicity are expected at these high masses (Bate 2005).

The slope at masses above $1 M_{\odot}$ should otherwise be more reliable, in view of the color excess and distance derived for the cluster, and the expected brightness range covered by these stars, which allow one to expect a higher degree of completeness in the cluster members detection. In this figure we note the present sequence of assigned candidate PMS members, with a mass function very well reproduced by a Salpeter mass function slope (-2.35 in the plot of the figure).

6.5. Comments on the age distribution

There are some cases in the recent literature of regions similar to this, where a central, ageing cluster has caused a set of structures around it, driving in some cases the formation of new stars (Yun et al. 2008; Deharveng et al. 2003). Here we could be witnessing a region similar to these, but some 10 million years later than those other regions.

In view of the possible presence of two generations of MS and post-MS stars in the central field, as suggested by our data in combination with isochrone fitting, we speculate that the bubble may have been shaped by the first generation of stars some 40 Myr ago. This population may be quite dispersed by now. The new generation, with ages approximately around 3-5 Myr found both for MS, post-MS, and PMS stars, may have been triggered by the first population, and although we see a cluster projected close to the centre of the bubble, its exact location may just as well be closer to the shell of the bubble in the line of sight towards us. As seen in Fig. 1 the red structures without bright rims at the edges, are most likely cloud filaments and structure located on the near side of the bubble, and would be showing absorption relative to the $H\alpha$ emission background. These structures contrast to the ones with bright rims, i.e. enhanced $H\alpha$ emission at the edges.

In this context, we may interpret the collection of Class I sources in the very direction of the cluster core. As suggested by P09, they could be indeed embedded in the above mentioned $H\alpha$ absorbing structure, and be a part of the surrounding region, where other star forming centers are, seen only in foreground.

All these indications enhance the view of S284 as a region with past events of star formation at different ages, and presently ongoing formation activity of new generations of stars, ranging in age from a few Myr down to very young objects in the first formation phases.

7. Summary and Conclusions

- We obtained deep UBVRJHK photometry in the central 6.5' part of the Dolidze 25 cluster, reaching the 10σ limiting magnitudes of $V = 23.3$, $J = 19.7$, and $K_S = 18.6$. Magnitudes, colours, and positions of all sources, as well as possible membership assignments, are published in Table 1, available on-line.
- The membership analysis revealed 214 candidate members, of which 35 are main-sequence or post-MS stars, and the rest are PMS candidates. The PMS candidates comprise optically selected sources as well as sources with IR excess.
- The use of low metallicity ZAMS and isochrones to estimate distance, gives a new distance for the cluster to be 3.6 kpc.
- The ages of the optically selected PMS stars are likely around 5 Myr and those of the IR-excess sources possibly slightly younger.
- We find a possible existence of two generations of member stars, one with MS and PMS stars of age below 5 Myr, and another older population of age around 40 Myr. The spatial distribution of the two potential generations is found to be distinct, giving independent support to this suggestion.
- Dolidze 25 seems to be located in the centre of an ionized bubble which probably originated from the older generation of stars. We cannot exclude that the young cluster generation is located in the near side of the bubble shell, though.

In the previous presentation of results we have described the presence of post-MS cluster members at similar luminosity but different evolutionary states, as inferred from their color indices. At the same time, we detect the presence of MS candidate members with masses below the presently PMS stars. This evidence adds to the indication of the presence in the field of a wide range in distances, with foreground and background groupings of stars (see Fig. 3) producing the general view of a region where star formation has been going on for a long time, both at different places of the HII region, and in the same place at different epochs. At present, we observe this mixture of populations, with a star forming process which takes place in an already formed cluster, giving rise to the presence of two star generations of different age and being members of the same cluster. The evolved state of some of the most luminous cluster members, together with the presence of low mass MS member stars, can indeed be interpreted in this context. We can not exclude, though, that the younger population is seen in projection in front of the older one, possibly being formed in the shell of the bubble. Finally, we recall that the interpretation of two generations of member stars is furthermore favoured from inspection of the spatial distribution.

Acknowledgements. The NOT staff astronomers Tapio Pursimo and John Telting are warmly acknowledged for the ALFOSC observations carried out during service/technical nights. Thanks to the referee, A. Moffat, for his comments and recommendations which resulted in an improvement of the article. We also wish

to tank D. Lennon for his very valuable and useful comments. The data presented here have been taken using ALFOSC, which is owned by the Instituto de Astrofísica de Andalucía (IAA) and operated at the Nordic Optical Telescope under agreement between IAA and the NBIFAFG of the Astronomical Observatory of Copenhagen. This work has been supported by the Spanish MICCIN through grants AYA2007-64052, and by the Consejería de Educación y Ciencia de la Junta de Andalucía, through TIC 101 and TIC 4075 grants. EJA acknowledges the financial support from the Spanish MICINN under the Consolider-Ingenio 2010 Program grant CSD2006-00070: First Science with the GTC. This research has made use of the SIMBAD database, operated at CDS, Strasbourg, France, the NASA ADS Abstract Service, and the WEBDA data base, developed by Jean-Claude Mermilliod at the Laboratory of Astrophysics of the EPFL (Switzerland), and further developed and maintained by Ernst Paunzen at the Institute of Astronomy of the University of Vienna (Austria). This publication makes use of data products from the Two Micron All Sky Survey, which is a joint project of the University of Massachusetts and the Infrared Processing and Analysis Center/California Institute of Technology, funded by the National Aeronautics and Space Administration and the National Science Foundation. We have also made use of the public data in the AAO/UKST H α survey.

References

- Alexander, M. J., Kobulnicky, H. A., Clemens, D. P., et al. 2009, *AJ*, 137, 4824
- Aller, L. H., Appenzeller, I., Baschek, B., et al. 1982, *Landolt-Börnstein: Numerical Data and Functional Relationships in Science and Technology - New Series* " Gruppe/Group 6 Astronomy and Astrophysics " Volume 2 Schaifers/Voigt: Astronomy and Astrophysics / Astronomie und Astrophysik " Stars and Star Clusters / Sterne und Sternhaufen, ed. L. H. Aller, I. Appenzeller, B. Baschek, H. W. Duerbeck, T. Herczeg, E. Lamla, E. Meyer-Hofmeister, T. Schmidt-Kaler, M. Scholz, W. Seggewiss, W. C. Seitter, & V. Weidemann
- Baraffe, I., Chabrier, G., Allard, F., & Hauschildt, P. H. 1998, *A&A*, 337, 403
- Barro, G., Gallego, J., Pérez-González, P. G., et al. 2009, *A&A*, 494, 63
- Bate, M. R. 2005, *MNRAS*, 363, 363
- Bhavya, B., Mathew, B., & Subramaniam, A. 2007, *Bulletin of the Astronomical Society of India*, 35, 383
- Cardelli, J. A., Clayton, G. C., & Mathis, J. S. 1989, *ApJ*, 345, 245
- Carlson, L. R., Sabbì, E., Sirianni, M., et al. 2007, *ApJ*, 665, L109
- Chen, L., de Grijs, R., & Zhao, J. L. 2007, *AJ*, 134, 1368
- Clark, J. S., Negueruela, I., Davies, B., et al. 2009, *A&A*, 498, 109
- Deharveng, L., Zavagno, A., Salas, L., et al. 2003, *A&A*, 399, 1135
- Delgado, A. J., Alfaro, E. J., & Yun, J. L. 2007, *A&A*, 467, 1397
- Delgado, A. J., González-Martín, O., Alfaro, E. J., & Yun, J. 2006, *ApJ*, 646, 269
- Delgado, A. J., Miranda, L. F., & Alfaro, E. J. 1999, *AJ*, 118, 1759
- Delgado, A. J., Miranda, L. F., Fernández, M., & Alfaro, E. J. 2004, *AJ*, 128, 330
- Fitzsimmons, A., Brown, P. J. F., Dufton, P. L., & Rolleston, W. R. J. 1992, in *Lecture Notes in Physics*, Berlin Springer Verlag, Vol. 401, *The Atmospheres of Early-Type Stars*, ed. U. Heber & C. S. Jeffery, 41–+
- Fu, J., Hou, J. L., Yin, J., & Chang, R. X. 2009, *ApJ*, 696, 668
- Golay, M., ed. 1974, *Astrophysics and Space Science Library*, Vol. 41, *Introduction to astronomical photometry*
- Kaas, A. A. 1999, *AJ*, 118, 558
- Kaas, A. A., Olofsson, G., Bontemps, S., et al. 2004, *A&A*, 421, 623
- Koornneef, J. 1983, *A&A*, 128, 84
- Landolt, A. U. 1992, *AJ*, 104, 340
- Larsen, S. S., Efremov, Y. N., Elmegreen, B. G., et al. 2002, *ApJ*, 567, 896
- Lejeune, T., Cuisinier, F., & Buser, R. 1998, *VizieR Online Data Catalog*, 413, 65
- Lejeune, T. & Schaerer, D. 2001, *A&A*, 366, 538
- Lennon, D. J., Dufton, P. L., Fitzsimmons, A., Gehren, T., & Nissen, P. E. 1990, *A&A*, 240, 349
- Lohmann, W. 1972, *Astronomische Nachrichten*, 294, 105
- Mermilliod, J.-C. 1982, *A&A*, 109, 37
- Moffat, A. F. J., Jackson, P. D., & Fitzgerald, M. P. 1979, *A&AS*, 38, 197
- Moffat, A. F. J. & Vogt, N. 1975, *A&AS*, 20, 85
- Pedicelli, S., Bono, G., Lemasle, B., et al. 2009, *A&A*, 504, 81
- Przybilla, N. 2008, *Reviews in Modern Astronomy*, 20, 323
- Przybilla, N., Nieva, M., & Butler, K. 2008, *ApJ*, 688, L103
- Puga, E., Hony, S., Neiner, C., et al. 2009, *A&A*, 503, 107
- Puga, E., Neiner, C., Hony, S., et al. 2007, in *IAU Symposium*, Vol. 237, *IAU Symposium*, ed. B. G. Elmegreen & J. Palous, 465–465
- Ripepi, V., Marconi, M., Palla, F., et al. 2006, *Memorie della Società Astronomica Italiana*, 77, 317
- Robin, A. C., Reylé, C., Derrière, S., & Picaud, S. 2003, *A&A*, 409, 523
- Sabbì, E., Sirianni, M., Nota, A., et al. 2007, *AJ*, 133, 44
- Sánchez Gil, M. C., Alfaro, E. J., & Pérez, E. 2009, *ApJ*, 702, 141
- Skrutskie, M. F., Cutri, R. M., Stiening, R., et al. 2006, *AJ*, 131, 1163
- Subramaniam, A., Mathew, B., Bhatt, B. C., & Ramya, S. 2006, *MNRAS*, 370, 743
- Turbide, L. & Moffat, A. F. J. 1993, *AJ*, 105, 1831
- Vandenberg, D. A. & Poll, H. E. 1989, *AJ*, 98, 1451
- Whittet, D. C. B. 1988, in *Dust in the Universe*, ed. C. Eiroa & K.-W. Hodapp, 25–53
- Yi, S., Demarque, P., Kim, Y.-C., et al. 2001, *ApJS*, 136, 417
- Yun, J. L., Djupvik, A. A., Delgado, A. J., & Alfaro, E. J. 2008, *A&A*, 483, 209